Performance Analysis for Multi-hop Cognitive Radio Networks with Energy Harvesting by Using Stochastic Geometry

Lu Ge, *Member, IEEE,* Gaojie Chen, *Senior Member, IEEE,* Yue Zhang, *Senior Member, IEEE,* Jie Tang, *Senior Member, IEEE,* Jintao Wang, *Senior Member, IEEE,* Jonathon A. Chambers, *Fellow, IEEE*

***Abstract*—Cognitive multi-hop relaying has been widely considered for device-to-device (D2D) communications for applications in the physical layer of the Internet of Things. In this paper, we construct a multi-hop cellular D2D communications system model with energy harvesting in underlay cognitive radio networks. The locations of primary user equipments PUEs and cellular base stations are considered as a Poisson point process in this model. The transmit power of secondary devices are collected from the power beacon with time-switching energy harvesting policy. Two charging policies for different applications are considered in the paper. Then, the end-to-end outage probability analysis expressions of these two scenarios for the transmission scheme subject to interferences from PUEs are derived. The optimal harvesting time ratio is obtained to get the maximum capacity for end-to-end D2D communications. The analytical results are validated by performing Monte Carlo simulation of the end-to-end outage probability, which is based on the half-duplex transmission scheme. The results of this paper provide a potential pathway to reduce reliance on grid or battery energy supplies, and hence, further strengthen the benefits for the environment and deployment of future smart devices.**

***Index Terms*—Cognitive networks, multi-hop, D2D, outage probability, energy harvest, stochastic geometry, Internet of Things**

I. Introduction

The Internet of Things (IoT) and the Tactile Internet have become essential research directions to accelerate the development of fifth generation (5G) mobile networks and beyond. IoT is a promising technology which aims to revolutionize and connect the global world via heterogeneous smart devices through seamless connectivity [1]. Massive IoT applications require an enormous number of connected smart devices, such as deployments in shipping environments, smart-homes (buildings), smart-cities, smart energy systems, and agricultural monitoring environments, etc., which need to update regularly to the cloud with a low end-to-end cost [2]–[5].

This work was supported by the National Key R&D Program of China (Grant No.2017YFE011230), EU Horizon 2020 project grant number 761992 (IoRL), and the Engineering and Physical Sciences Research Council(EPSRC) funding EP/R006377/1 (M3NETs).

L. Ge, G. Chen, Y. Zhang (Corresponding Author) and Jonathon A. Chambers are with Department of Engineering, University of Leicester, Leicester, LE1 7RH, U.K. (E-mail:lu.ge, gaojie.chen, yue.zhang and jonathon.chambers@le.ac.uk)

J. Tang is with the School of Electronic and Information Engineering, South China University of Technology, Guangzhou, China.(E-mail:eejtang@scut.edu.cn)

J. Wang is with the Department of Electronic Engineering, Tsinghua University, Beijing, 100084 China.(E-mail:wangjintao@tsinghua.edu.cn)

Cognitive radio (CR) technology is available to provide the opportunity for unlicensed users (secondary users) to share the wireless spectrum without the need for expensive spectrum licenses as long as the secondary users can protect the data of licensed users (primary users) [6]. Existing wireless networks such as wireless sensor networks also benefit from CR technology by integrating it into their existing infrastructure. The CR network has three paradigms: underlay, overlay and interweave [7]. In the underlay mode, if the interference caused by the transmission frequency of the secondary device to the primary device is strictly controlled, the secondary device can transmit with the same frequency as the primary one [8]–[10]. The overlay pattern allows the secondary devices to transmit by adopting the same frequency spectrum as the primary devices. However, the premise is that the channel state information is known between the primary and secondary devices, and secondary devices use part of transmit power to communicate with each other; in the meanwhile, the remaining transmit power of the secondary devices is used to support the transmission of primary devices. The authors of [11] investigated simultaneous wireless information and power transfer in a cooperative overlay spectrum sharing system, and exact expressions for user outage probability for primary users was also provided. In addition, in interleaved communication systems, CR can also transmit signals using spectral holes so as not to interfere with other communications [12].

Device-to-device (D2D) communications has been considered as one of the key technologies in a 5G cellular network, and relates to direct transmission between devices [13]–[16]. D2D communications can improve spectrum efficiency, reduce power consumption, and efficiently offload traffic from the base station/access points [17]. In [18], a cross-cell fractional reuse-based frequency resource multiplexing scheme was proposed for multi-cell D2D communications to reduce interference between adjacent cells. In order to obtain a better access probability, secondary users are treated as relays to enhance the primary users in [19]. In [20], the authors optimized the transmission rate of the D2D users when modelling D2D users as cognitive secondary users. A full-duplex relay-assisted D2D communications system was proposed in [21], and the exact closed-form expression for the outage probability was obtained. In [22] the energy efficiency of the D2D users has been maximized according to the minimum rate requirement of the D2D users and the cellular users. In addition, cooperative D2D communications in an uplink cellular network was investigated

in [23]; and the optimal spectrum and power allocation were obtained to maximize the total average achievable rate. From the perspective of IoT network architecture, the exchange of information between two IoT devices usually requires relay assistance [24]. Therefore, one of the common evaluations for the performance of D2D communication systems is to undertake end-to-end performance analysis. In [25], the authors have quantified the system throughput and energy efficiency with the average transmission time to investigate the end-to-end outage performance. In [26], the authors stated that the connectivity of a path can be used for the determination of the maximum end-to-end outage probability in the context of the route selection.

Energy harvesting (EH) is an emerging technology for enabling green, sustainable, and autonomous wireless networks. In particular, radio frequency (RF) energy harvesting provides key benefits in wireless transmission. However, one of the barriers to connect massive smart devices is supplying sufficient energy to operate the network in a self-sufficient manner whilst maintaining the quality of service [27]. Recent research has shown that a combination of different energy harvesting schemes, such as time splitting, power splitting, and antenna switching, can be utilized to collect the energy for the devices [28]. The time-splitting protocol means the receiver at the device switches over time between harvesting energy device and decoding information, whereas the power splitting protocol means that part of the received signal is used for EH and the rest is used for information processing in [29], [30]. In this paper, a time-splitting scheme is employed to collect energy of the D2D secondary devices since such time splitting is known to require less complex circuitry [31]. Two charging strategies are proposed based on the time-splitting protocol, one for identical charging channels and the other for varying charging channels. Both of these charging strategies can effectively charge the device during the cognitive massive D2D connections based on different deployment scenarios. Furthermore, these two charging strategies are able to act as the baselines, which enable the development of a high energy-efficiency network in the near future, such as one having the ability to support battery-free IoT devices [32]. In [33], the authors proposed combined energy management for queuing control to deal with the delay requirements of tactile communication in the presence of energy constraints on IoT devices.

Currently, stochastic geometry is an important mathematical tool for analysing large scale ad hoc, cognitive and cellular networks [34]. In [35], a model for cognitive D2D communications was presented using RF energy harvesting from the ambient interference in a multi-channel cellular network, and stochastic geometry was used to analyse and evaluate the outage probabilities of the system. The authors of [36] investigated a power transfer model and an information signal model to realize energy harvesting and secure information transmission. Energy harvesting applications with multi-hop communications and optimization of energy harvesting time have also not been considered.

In this paper, we model a multi-hop D2D cognitive radio network with a time-splitting energy harvesting scheme. The transmit power of secondary devices is determined by jointly considering the mutual constraint of the preset maximum transmit power, peak interference power and the amount of energy harvesting. And then, the end-to-end outage probability of the proposed multi-hop D2D cognitive system is analyzed. The main contributions are listed as below:

- Building a multi-hop cognitive D2D communications system model with energy harvesting, where the locations of the PUEs and primary base stations (PBSs) are represented by a homogeneous Poisson point process (PPP).
- Proposing two charging policies, one is for identical charging channels and the other is for varying charging channels. After that, this article analyzes the end-to-end outage probability for the multi-hop CR D2D communications by considering the interference from the PUEs and PBSs.
- Deriving the optimal charging time ratio to maximize the end-to-end transmission rate of the proposed system.
- Performing Monte Carlo simulations to validate the proposed system, and confirming that the simulation results match with the theoretical expressions.

The structure of the remaining part of the paper is organised as follows: Section II introduces the proposed cellular D2D communications with energy harvesting in cognitive radio networks. Section III presents two energy harvesting strategies regarding different scenarios. Section IV provides the theoretical analysis of end-to-end outage probability. Section V shows the optimisation of energy harvesting time ratio. Section VI presents all numerical simulation results along with discussions to verify the rationality of the proposed system. All outcomes of this study are summarized in Section VII, and abbreviations and notifications for the paper are listed in Table I.

TABLE I
SYMBOL AND DEFINITION USED

Symbol/Abbreviation	Definition/Explanation
5G	Fifth generation
BS	Base station
CDF	Cumulative distribution function
CR	Cognitive radio
PUE	Primary users equipment
PBS	Primary base station
D2D	Device-to-device
DF	Decode-and-forward
EH	Energy harvesting
HD	Half-duplex
IoT	Internet of Things
PB	Power beacon
PDF	Probability density function
PPP	Poisson point process
RF	Radio frequency
λ_B and λ_C	Density of PBSs and PUEs
α	Path loss exponent
$\mathbb{E}(\cdot)$	Expectation operator
$\mathbb{P}(\cdot)$	Probability operator
$\mathrm{sinc}(\cdot)$	Sinc function
$\Gamma(\cdot)$	Gamma function
$\|\cdot\|^2$	Distance operation

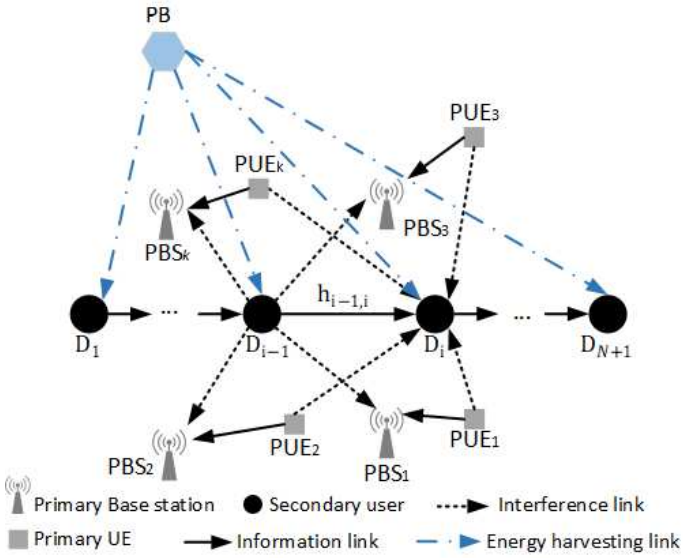

Fig. 1. System model of the buffer-aided link selection in multi-relay cooperative networks.

II. System Model

A cognitive radio multi-hop D2D communications system with energy harvesting is shown in Fig. 1, where the signal is sent from the secondary source device D_1 to the secondary destination device D_{N+1} with N hops by adopting the decode-and-forward transmission scheme. The signal is transmitted from secondary devices to PBSs and PUEs and the signal received at the secondary devices from PBSs and PUEs are treated as interference. The locations of the PBSs and the PUEs are modelled as homogeneous PPPs Φ_B and Φ_C with densities λ_B and λ_C, respectively. All secondary devices are equipped with a half-duplex antenna, so that each secondary device cannot simultaneously transmit and receive the signal. We assume that all secondary devices are powered by a fixed power beacon (PB).

We assume independent Rayleigh fading channel models with path loss. The channel coefficients can be expressed as $h_{m,n} = \beta_{m,n} d_{m,n}^{-\alpha/2}$, where $d_{m,n}$ and α represent the distance and the pathloss exponent between two devices, m and n, respectively. $\beta_{m,n}$ is a complex Gaussian random variable with unit variance. Therefore, $|h_{m,n}|^2$ is the channel gain and $\mathbb{E}[|h_{m,n}|^2] = d_{m,n}^{-\alpha}$ is defined as the average channel power.

Assuming that before the signal is passed to the next secondary device, the current secondary device and all remaining secondary devices receive energy from the PB. Moreover, since the time splitting scheme is used, the EH phase takes place during time ratio τ_i $(0 < \tau_i < 1)$, where i is the index of the secondary devices. In this paper, we assume $\tau_i = \tau, for\ \forall i \in \{1, 2, \cdots, N+1\}$. The harvested power at the ith secondary device is given by

$$\overline{P}_{D_i} = \frac{\eta P_T \tau \sum_{j=1}^{i} |h_{p,i,j}|^2}{d_{p,i}^{\alpha}(1-\tau)}, \tag{1}$$

where $\eta \in (0,1)$ denotes the energy harvesting efficiency dependent on the design of an efficient rectifier [37] and j represents the number of times of charging at the ith secondary device. P_T is the transmit power at the PB. $d_{p,i}$ is the distance between the PB and ith secondary device.

In actual deployment, the transmitted signal power cannot exceed the rated power P_{max}, and if it exceeds P_{max}, it can only be transmitted at P_{max}. For the underlay CR networks, the secondary device uses the same spectrum band as the primary device to transmit signals, therefore, the transmit power of the secondary device must be less than the peak interference power at the PBSs. Thus, it is necessary to consider comprehensively the constraints of the peak interference power I_{th} at the PBSs, the rated power P_{max} and the total harvested transmit energy $\overline{P}_{D_i}$. The transmit power of the ith secondary device should satisfy the following constraint

$$P_{D_i} = \min\left(\frac{I_{th}}{\max\limits_{b\in\Phi_B}\left(\frac{|h_{i,b}|^2}{d_{i,b}^{\alpha}}\right)}, \overline{P}_{D_i}, P_{max} \right), \tag{2}$$

where $d_{i,b}$ and $h_{i,b}$ denote the distance and the channel coefficient between the ith secondary device and the PBSs, respectively. The received signal at D_i from D_{i-1} can be expressed as

$$y_{D_i} = \frac{\sqrt{P_{D_{i-1}}} h_{i-1,i}}{d_{i-1,i}^{\alpha/2}} x_{i-1} + \sum_{c\in\Phi_C} \left(\frac{\sqrt{P_c} h_{c,i}}{d_{c,i}^{\alpha/2}} \right) x_c + n_i, \tag{3}$$

where $h_{i-1,i}$ and $d_{i-1,i}$ represent the coefficient of the channel and the distance between two secondary devices, respectively; $h_{c,i}$ and $d_{c,i}$ denote the channel coefficient and the distance between PUEs and the ith secondary device. x_{i-1} is the signal sent from D_{i-1} to D_i, and x_c is the interference signal from the PUEs. P_c denotes the transmit power of the PUEs. n_i is the additive white Gaussian noise (AWGN) at D_i with variance σ_n^2, which is normalized to unity. As a result, the SINR at the ith secondary device can be expressed as

$$\gamma_{D_i} = \frac{\min\left(\frac{I_{th}}{\max\limits_{b\in\Phi_B}\left(\frac{|h_{i,b}|^2}{d_{i,b}^{\alpha}}\right)}, \overline{P}_{D_i}, P_{max} \right) \frac{|h_{i-1,i}|^2}{d_{i-1,i}^{\alpha}}}{\sum\limits_{c\in\Phi_C}\left(P_c \frac{|h_{c,i}|^2}{d_{c,i}^{\alpha}}\right) + 1}. \tag{4}$$

The proposed EH strategies will be presented in the next section.

III. Energy Harvesting Strategies

In this section, two charging scenarios are proposed. The effect of charging link on the energy term $\overline{P}_{D_i}$ are considered.

- *Case1: identical charging channels*
  For this case, the channels between PB and the ith

secondary device are assumed to be unchanged regardless of the hops, $h_{p,i,j} = h_{p,i}, \forall j \in \{1, 2, \cdots, N+1\}$, which can be considered as block fading channels [38]. The cumulative distribution function (CDF) of $\overline{P}_{D_i}$ is

$$\begin{aligned} F_{\overline{P}_{D_i}}(z) &= \mathbb{P}\left(\frac{\eta P_T \tau i |h_{p,i}|^2}{d_{p,i}^{\alpha}(1-\tau)} < z\right) \\ &= 1 - \exp\left(-\frac{z d_{p,i}^{\alpha}(1-\tau)}{i P_T \tau \eta}\right). \end{aligned} \tag{5}$$

The probability density function (PDF) of $\overline{P}_{D_i}$ is obtained as

$$f_{\overline{P}_{D_i}}(z) = \frac{z d_{p,i}^{\alpha}(1-\tau)}{i P_T \tau \eta} \exp\left(-\frac{z d_{p,i}^{\alpha}(1-\tau)}{i P_T \tau \eta}\right). \tag{6}$$

- *Case2: varying charging channels*
The channels between PB and the ith secondary device are changed with hops in this case. This application scenario can be used in the real-time geometry-based channel emulator in [39]. The CDF of $\overline{P}_{D_i}$ can be expressed as follows

$$\begin{aligned} F_{\overline{P}_{D_i}}(z) &= \mathbb{P}\left(\frac{\eta \tau P_t \sum_{j=1}^{i} |h_{p,i,j}|^2}{d_{p,i}^{\alpha}(1-\tau)} < z\right) \\ &= \mathbb{P}\left(\sum_{j=1}^{i} |h_{p,i,j}|^2 < \frac{z}{K}\right) \\ &= \frac{\gamma(i, \frac{z}{K})}{\Gamma(i)}, \end{aligned} \tag{7}$$

where according to the definition of the CDF of the regularized Gamma distribution $F_{\overline{P}_{D_i}}(z; i, K) = \int_0^z f(u; i, K) du = \frac{\gamma(i, \frac{z}{K})}{\Gamma(i)}$, and $\gamma(i, \frac{z}{K})$ is the lower incomplete Gamma function. The term $K = \frac{\eta \tau P_t}{d_{p,i}^{\alpha}(1-\tau)}$ and $\Gamma(i) = (i-1)!$ is the Gamma function. Then, the PDF of $\overline{P}_{D_i}$ can be written as

$$f_{\overline{P}_{D_i}}(z) = \frac{\left(\frac{d_{p,i}^{\alpha}}{\eta P_T \tau}\right)^i z^{i-1} \exp\left(-\frac{d_{p,i}^{\alpha} z}{\eta P_T \tau}\right)}{(i-1)!}. \tag{8}$$

Based on the proposed system model with different EH strategies, the theoretical analysis of the end-to-end outage probability will be given in the next section.

IV. Outage Probability Analysis

Based on the above charging scenarios proposed in the last section, we derive the end-to-end outage probability for these two EH scenarios. The definition of outage event between the $(i-1)$th secondary device and ith secondary device is given by

$$\mathbb{P}_{i-1,i}^{out} = \mathbb{P}\left(\frac{\min\left(\frac{I_{th}}{\max\limits_{b \in \Phi_B}\left(\frac{|h_{i,b}|^2}{d_{i,b}^{\alpha}}\right)}, \overline{P}_{D_i}, P_{max}\right) \frac{|h_{i-1,i}|^2}{d_{i-1,i}^{\alpha}}}{\sum\limits_{c \in \Phi_C}\left(P_c \frac{|h_{c,i}|^2}{d_{c,i}^{\alpha}}\right) + 1} < R\right), \tag{9}$$

where $R = 2^{R_{th}} - 1$, and R_{th} is the target rate. Letting $A = \max\limits_{b \in \Phi_B}\left(\frac{|h_{i,b}|^2}{d_{i,b}^{\alpha}}\right)$ and $D = \frac{\frac{|h_{i-1,i}|^2}{d_{i-1,i}^{\alpha}}}{\sum\limits_{c \in \Phi_C}\left(P_c \frac{|h_{c,i}|^2}{d_{c,i}^{\alpha}}\right)+1}$, the CDF of A can be first obtained by using the probability generating functional lemma as

$$\begin{aligned} F_A(\omega) &= \mathbb{P}\left(\max_{b \in \Phi_B}\left(\frac{|h_{i,b}|^2}{d_{i,b}^{\alpha}} < \omega\right)\right) \\ &= \mathop{\mathbb{E}}_{b \in \Phi_B}\left[\prod_{b \in \Phi_B} e^{-d_{i,b}^{\alpha}\omega}\right] \\ &= \exp\left(-\rho_B \int_0^{2\pi}\int_0^{\infty} r e^{-r^{\alpha}\omega} \mathrm{d}r\mathrm{d}\theta\right) \\ &= \exp\left(-\omega^{-\frac{2}{\alpha}}\psi\right), \end{aligned} \tag{10}$$

where $\psi = \frac{2\pi\rho_B}{\alpha}\Gamma(\frac{2}{\alpha})$, and $\Gamma(\cdot)$ is the gamma function. Therefore, the PDF of A can be given as

$$f_A(\omega) = \omega^{-\frac{2}{\alpha}-1}\frac{2\psi}{\alpha}\exp\left(-\omega^{-\frac{2}{\alpha}}\right). \tag{11}$$

The CDF of D can be expressed as

$$\begin{aligned} F_D(\mu) =& \mathbb{P}\left(\frac{\frac{|h_{i-1,i}|^2}{d_{i-1,i}^{\alpha}}}{\sum\limits_{c \in \Phi_C}\left(P_c \frac{|h_{c,i}|^2}{d_{c,i}^{\alpha}}\right)+1} < \mu\right) \\ =& 1 - \exp(-\mu d_{i-1,i}^{\alpha})\mathbb{E}_{\Phi_C}\left[\prod_{c \in \Phi_C} e^{-yP_C|h_{c,i}|^2 d_{i-1,1}^{\alpha} d_{c,i}^{-\alpha}}\right] \\ \overset{(a)}{=}& 1 - \exp(-\mu d_{i-1,i}^{\alpha}) \\ & \times \mathbb{E}_{\Phi_C}\left[\prod_{c \in \Phi_C}\int_0^{\infty} e^{-\mu P_C k d_{i-1,1}^{\alpha} d_{c,i}^{-\alpha}} e^{-k} \mathrm{d}k\right] \\ =& 1 - \exp(-\mu d_{i-1,i}^{\alpha})\mathbb{E}_{\Phi_C}\left[\prod_{c \in \Phi_C}\frac{1}{1 + P_C \mu (\frac{d_{i-1,i}}{d_{c,i}})^{\alpha}}\right] \\ \overset{(b)}{=}& 1 - \exp(-\mu d_{i-1,i}^{\alpha}) \\ & \times \exp\left(\rho_C \int_0^{2\pi}\int_0^{\infty}\left(\frac{-P_C \mu (\frac{d_{i-1,i}}{r})^{\alpha}}{1 + P_C \mu (\frac{d_{i-1,i}}{r})^{\alpha}}\right) r \mathrm{d}r\mathrm{d}\theta\right) \\ =& 1 - \exp(-\mu d_{i-1,i}^{\alpha})\exp(-\mu^{\frac{2}{\alpha}}\Omega_i), \end{aligned} \tag{12}$$

where setting $k = |h_{i-1,i}|^2$ at (a), so the PDF of k should be $f_k(k) = e^{-k}$ and for (b), it holds for the probability generating functional; and then $\Omega_i = \frac{\pi d_{i-1,i}^2 \rho_c P_c^{\frac{2}{\alpha}}}{P_T^{\frac{2}{\alpha}} \mathrm{sinc}(\frac{2}{\alpha})}$. Therefore, the PDF of D can be obtained as

$$f_D(\mu) = \left(\frac{2\Omega_i}{\alpha}\mu^{\frac{2}{\alpha}-1} + d_{i-1,i}^{\alpha}\right)\exp\left(-\mu d_{i-1,i}^{\alpha} - \mu^{\frac{2}{\alpha}}\Omega_i\right). \tag{13}$$

From the above mathematical derivation of SINR γ_{D_i}, the outage probability in (9) can be obtained as

$$\begin{aligned}\mathbb{P}_{i-1,i}^{out} =&\mathbb{P}(\gamma_{D_i} < R)\\ =&\mathbb{P}\left(\left(\min\left(\frac{I_{th}}{A}, P_{D_i}, P_{max}\right)D\right) < R\right)\\ &+\mathbb{P}\left(P_{max}D < R | P_{max} < \min\left(\frac{I_{th}}{A}, P_{D_i}\right)\right)\\ &+\mathbb{P}\left(P_{D_i}D < R | P_{max} < \min\left(\frac{I_{th}}{A}, P_{max}\right)\right)\\ &+\mathbb{P}\left(\frac{I_{th}}{A}D < R | P_{max} < \min\left(P_{D_i}, P_{max}\right)\right)\\ =&\int_0^{\frac{I_{th}}{P_{max}}}\int_{\frac{I_{th}}{y}}^{\infty}\int_0^{\frac{R}{P_{max}}} f_D(t)f_{P_{D_i}}(x)f_A(y)\mathrm{d}t\mathrm{d}x\mathrm{d}y\\ &+\int_C^{\infty}\int_0^{\frac{I_{th}}{x}}\int_0^{\frac{R}{P_{max}}} f_D(t)f_A(y)f_{P_{D_i}}(x)\mathrm{d}t\mathrm{d}y\mathrm{d}x\\ &+\int_{\frac{I_{th}}{P_{max}}}^{\infty}\int_0^{\frac{I_{th}}{y}}\int_0^{\frac{R}{x}} f_D(t)f_{P_{D_i}}(x)f_A(y)\mathrm{d}t\mathrm{d}x\mathrm{d}y\\ &+\int_0^{\frac{I_{th}}{P_{max}}}\int_0^{P_{max}}\int_0^{\frac{R}{x}} f_D(t)f_{P_{D_i}}(x)f_A(y)\mathrm{d}t\mathrm{d}x\mathrm{d}y\\ &+\int_0^{P_{max}}\int_{\frac{I_{th}}{x}}^{\infty}\int_0^{\frac{Ry}{I_{th}}} f_D(t)f_A(y)f_{P_{D_i}}(x)\mathrm{d}t\mathrm{d}y\mathrm{d}x\\ &+\int_{\frac{I_{th}}{P_{max}}}^{\infty}\int_{P_{max}}^{\infty}\int_0^{\frac{Ry}{I_{th}}} f_D(t)f_{P_{D_i}}(x)f_A(y)\mathrm{d}t\mathrm{d}x\mathrm{d}y.\end{aligned} \tag{14}$$

The outage probability between $i-1$th secondary device and ith secondary device for EH case 1 and case 2 can be obtained as

$$\begin{aligned}\mathbb{P}_{i-1,i}^{out(\Psi)} =&\frac{4\pi\rho_B\Gamma\left(\frac{2}{\alpha}\right)\left(-\frac{d_{p,i}^{\alpha}(\tau-1)}{P_b\tau\eta}\right)^i}{\alpha^2\Gamma(i)}\\ &\times\left(\int_0^{\frac{I_{th}}{P_{max}}}\int_{\frac{I_{th}}{y}}^{\infty} W_1^{\Psi}(x,y)\mathrm{d}x\mathrm{d}y\right.\\ &+\int_{P_{max}}^{\infty}\int_0^{\frac{I_{th}}{x}} W_1^{\Psi}(x,y)\mathrm{d}y\mathrm{d}x\\ &+\int_{\frac{I_{th}}{P_{max}}}^{\infty}\int_0^{\frac{I_{th}}{y}} W_2^{\Psi}(x,y)\mathrm{d}x\mathrm{d}y\\ &+\int_0^{\frac{I_{th}}{P_{max}}}\int_0^{P_{max}} W_2^{\Psi}(x,y)\mathrm{d}x\mathrm{d}y\\ &+\int_0^{P_{max}}\int_{\frac{I_{th}}{x}}^{\infty} W_3^{\Psi}(x,y)\mathrm{d}y\mathrm{d}x\\ &\left.+\int_{\frac{I_{th}}{P_{max}}}^{\infty}\int_{P_{max}}^{\infty} W_3^{\Psi}(x,y)\mathrm{d}x\mathrm{d}y\right),\end{aligned} \tag{15}$$

The derivations of $W_1^{\Psi}(x,y)$, $W_2^{\Psi}(x,y)$, $W_3^{\Psi}(x,y)$, $\Psi \in \{C_1, C_2\}$, can be found in Appendix I. Although the general closed-form expressions for case 1 and case 2 cannot be given, the numerical results can be implemented by MATLAB [40]. By using the DF scheme, the end-to-end outage probability of the proposed system can be obtained as

$$\mathbb{P}_{e2e}^{out(\Psi)} = 1 - \prod_{i=1}^{N+1}\left(1 - \mathbb{P}_{i-1,i}^{out}\right). \tag{16}$$

The discussion of the optimization of EH time for two EH strategies will be given in the next section.

V. Optimal energy harvesting time

The EH time plays an essential role in the time-switching scheme because of its influence on system capacity. From the perspective of providing the potential pathway to reduce battery energy supplies, the EH time for each independent hop should be optimized when the system achieves maximum capacity. The nonlinear cost function for optimal time ratio can be mathematically expressed as follows,

$$\begin{aligned}&arg\max_{\boldsymbol{\tau}}\,(Cap)\\ &s.t.\quad 0<\tau_i<1,\quad \forall i\in\{1,2,\cdots,N+1\},\end{aligned} \tag{17}$$

where, the capacity of the system is given as

$$Cap = \frac{1-\tau}{N}\log_2\left(1+\frac{\frac{\eta P_T\sum_{i=1}^{N}\tau|h_{p,i,j}|^2}{d_{p,i}^{\alpha}(1-\tau)}\frac{|h_{i-1,i}|^2}{d_{i-1,i}^{\alpha}}}{\sum_{c\in\Phi_C}\left(P_c\frac{|h_{c,i}|^2}{d_{c,i}^{\alpha}}\right)+1}\right). \tag{18}$$

A. The optimization of EH time ratio for case 1

In case 1, we assume that the charging links remain unchanged for each charging process. The second order derivative of Cap can be obtained as

$$Cap_1^{''} = \frac{{\phi_1}^2}{N(\tau-1)\ln(2)\left(1+(\phi_1-1)\tau\right)^2}, \tag{19}$$

where $\phi_1 = \frac{\frac{\eta P_T N|h_{p,i,j}|^2}{d_{p,i}^{\alpha}}\frac{|h_{i-1,i}|^2}{d_{i-1,i}^{\alpha}}}{\sum_{c\in\Phi_C}(P_c\frac{|h_{c,i}|^2}{d_{c,i}^{\alpha}})+1}$.

B. The optimization of EH time ratio for case 2

In case 2, the charging links are changed for each charging process, therefore, we can obtain the second order derivative of Cap as follows

$$Cap_2^{''} = \frac{{\phi_2}^2}{N(\tau-1)\ln(2)\left(1+(\phi_2-1)\tau\right)^2}, \tag{20}$$

where $\phi_2 = \frac{\frac{\eta P_T\sum_{i=1}^{N}|h_{p,i,j}|^2}{d_{p,i}^{\alpha}}\frac{|h_{i-1,i}|^2}{d_{i-1,i}^{\alpha}}}{\sum_{c\in\Phi_C}(P_c\frac{|h_{c,i}|^2}{d_{c,i}^{\alpha}})+1}$.

Through mathematical operations for both two cases above, it is worth noting that the term $\tau-1$ is a negative and the other term is positive. Therefore, the above second order derivatives of the objective function is less than zero so the unique concave point can be found for both cases. The optimal harvesting time ratio is determined by the CVX function for different numbers of hops as shown in Table II and Table III.

TABLE II
CASE1: OPTIMAL ENERGY HARVESTING TIME RATIO FOR INCREASING NUMBERS OF HOPS

NO. of Hops	Max. Capacity	Optimal time ratio
2	4.738	0.25
3	4.311	0.22
5	3.093	0.19

TABLE III
CASE2: THE OPTIMAZATION OF HARVESTING TIME RATIO FOR INCREASING NUMBERS OF HOPS

NO. of Hops	Max. Capacity	Optimal time ratio
2	3.942	0.43
3	3.584	0.35
5	2.787	0.27

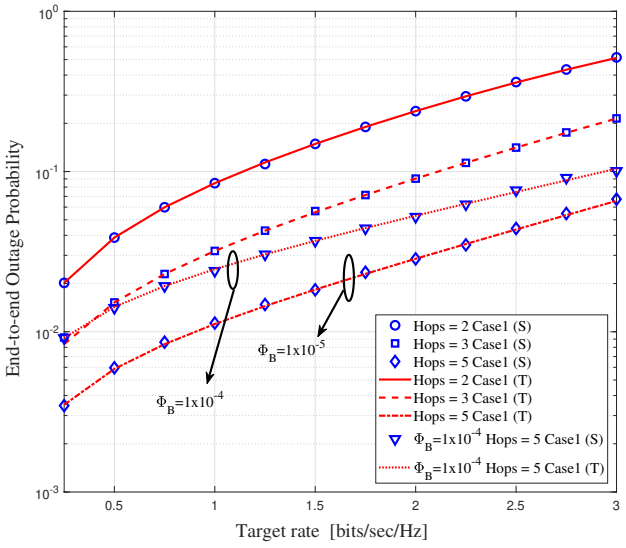

Fig. 2. Comparison of theoretical and numerical end-to-end outage probability with target rate for case 1.

VI. SIMULATION RESULTS

In this section, the simulation and theoretical results are given to verify the accuracy of our analysis. In excess of 10^5 independent Monte Carlo simulations introduce the following results. First, the noise power is assumed to be unity, and the path loss exponent of α equals to 4. The maximum rated transmit power P_{max} to noise ratio of each secondary device is set to 50 dB[1]. Additionally, the interference power cannot exceed I_{th} and is set to equal to 0.05. The energy harvesting efficiency is assumed as 0.5. The location of all secondary devices are fixed from $(-4, 0)$ to $(2, 0)$, respectively. All theoretical results are represented by a curve with denoted T, and simulation results are represented by various hollow shapes denoted as S.

A. Results for case 1

Fig. 2 demonstrates the variation of end-to-end outage probabilities with respect to varying system target rates. Both

[1]In reality, this is a tuning variable which can be adjusted, either higher or lower, according to real-world applications requirement.

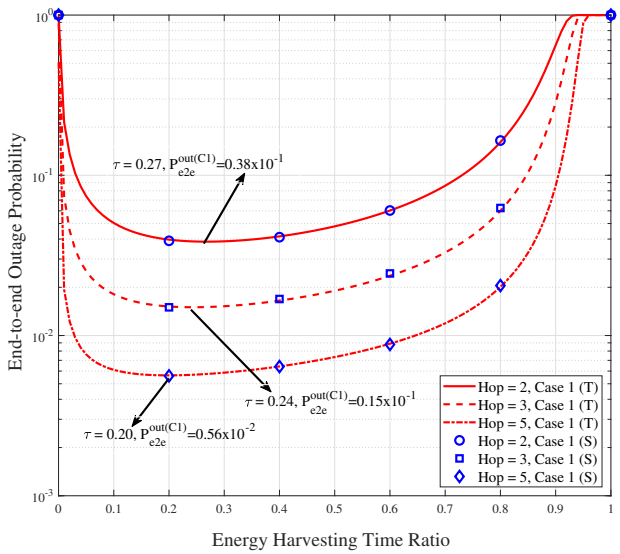

Fig. 3. The comparison of theoretical and numerical the end-to-end outage probability with EH time ratio for case 1.

simulations and theoretical results match. Furthermore, the power beacon supplies 30 dB power to the whole system continuously. The density of PUEs Φ_C and the density of cellular base stations Φ_B are both set to 1×10^{-5} m^{-2}. The end-to-end outage probability is increasing while the target rate increases. As the number of hops increases, the end-to-end outage probability of the system decreases. When the target rate achieves 2 bits/sec/Hz, the end-to-end probability of 2-hop system is 0.2383, the end-to-end probability of 3-hop system is 0.0903, and the end-to-end probability of 5-hop system drops to 0.0285. In order to demonstrate the effect of the density of PBSs on the end-to-end outage probability, the simulation and theoretical results for 5 hops at $\Phi_B = 1 \times 10^{-4}$ m^{-2} are also presented in this figure. Due to the density of PBSs increase, the interference power increases. As a result, the end-to-end probability increases.

In order to assess the influences of energy harvesting time on the system performance of case 1, Fig. 3 indicates the variation of end-to-end outage probability in terms of the EH time ratio. The optimal EH time ratio and the corresponding end-to-end outage probability are marked in Fig. 3. This optimal EH time ratio was obtained in Section V. It shows that the end-to-end probability is reduced when the number of hops is increasing. For example, when $\tau = 0.6$, the end-to-end outage probability of 2-hop system is 0.0603, similarly, the end-to-end outage probability of 3-hop system and 5-hop system are 0.0244 and 0.0088, respectively. Beyond this point, end-to-end outage probability is increasing dramatically as the time ratio increases. When the harvesting time is increasing, the secondary devices can collect more energy. However, due to the constraints of peak interference power and rated power, only a proportion of the harvested energy is effectively used. Additionally, the charging time ratio gradually increases, the term $1 - \tau$ will gradually decrease in (9), resulting in an increase in the target SINR and an increase in the probability

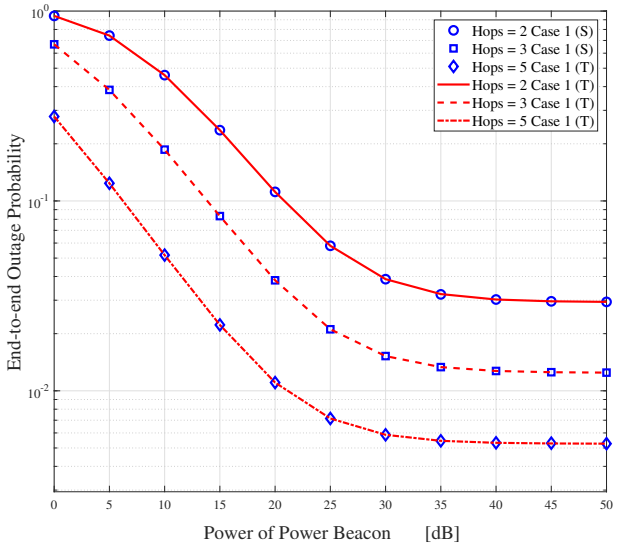

Fig. 4. The comparison of theoretical and numerical the end-to-end outage probability with power of power beacon for case 1.

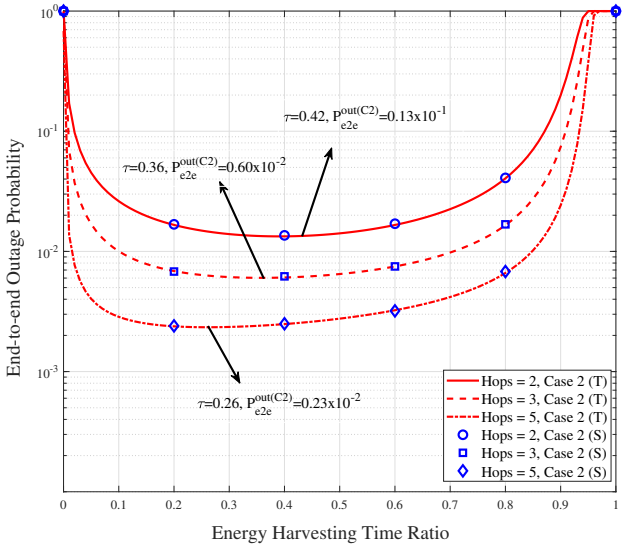

Fig. 6. Comparison between theoretical and numerical for end-to-end outage probability with EH time ratio for case 2.

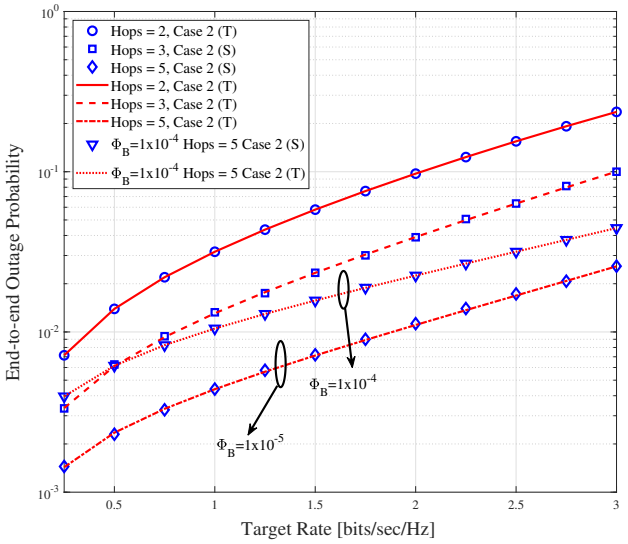

Fig. 5. Comparison of theoretical and numerical end-to-end outage probability with target rate for case 2.

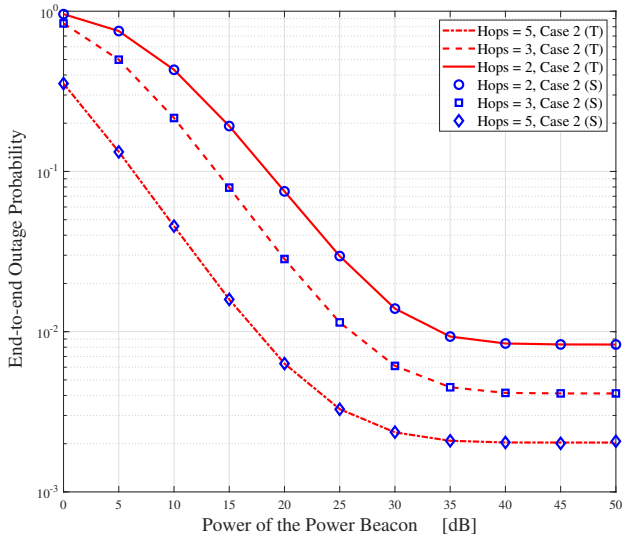

Fig. 7. Comparison of theoretical and numerical end-to-end outage probability with power of the power beacon for case 2.

of the final interruption.

In Fig. 4, the simulation and theoretical results of the end-to-end outage probability for each hop scenario are indicated with respect to the power variation of the power beacon. In general, when the power is more than 40 dB, the system end-to-end outage probability tends to be stable. It is because the transmit power of the secondary devices is limited by the interference power and the rated transmit power.

B. Results for case 2

Fig. 5 shows the comparison of end-to-end outage probability for different densities of PUEs and PBSs versus the target rate. We assumed that the density of PUEs Φ_C and the density of cellular base stations Φ_B are both set to 1×10^{-5} m^{-2} . It is shown that the end-to-end outage probability is increasing, when the target rate is increasing. For instance, the end-to-end probability of 2-hop system is 0.0973 when the target rate is 2 bits/sec/Hz, similarly, when the number of hops is increased to 3, the end-to-end probability is 0.0391 and when the number of hops is increased to 5, the end-to-end probability is reduced to 0.011. Moreover, a larger number of hops leads to a lower end-to-end outage probability trend. The increased PBSs density leads to an increased interference power, and hence, increases the end-to-end outage probability. For instance, the end-to-end probability is higher while the density of PBSs is 1×10^{-4} m^{-2}, compare to the density of

PBSs is 1×10^{-5} m^{-2}

To assess the impact of the energy harvesting time ratio of system performance, Fig. 6 represents the variation of the end-to-end outage probability in terms of harvesting time ratio. The simulation and theoretical results are perfectly matched. When the harvesting time ratio is from 0.3 to 1, although the secondary devices can harvest more energy, the effective usable energy is limited due to the defined constraints in this paper. Moreover, the transmission time ratio is reduced so that the end-to-end outage probability increases dramatically due to increasing the target SINR in (9). In details, when the EH time ratio achieves 0.8, for the 2-hop, 3-hop and 5-hop, the end-to-end outage probability are 0.0409, 0.0168, and 0.0068, respectively.

In Fig. 7, the simulation and theoretical results of end-to-end outage probability for each hop scenario are given as a function of the power variation of the power beacon. It clearly shows that by having a fixed power of the power beacon, the end-to-end probabilities of the proposed system are reduced with increasing the number of hops. The numerical integration results are correspond exactly with the simulation results. When the power is more than 40 dB, the system end-to-end outage probability tends to be stable, which means that the system always maintains the best performance while other parameters are unchanged. Besides, the variation of the hop number has no effect upon this stabilized point.

VII. Conclusion

In this paper, a multi-hop underlying CR D2D communications system with energy harvesting was constructed. This proposed model took into account the influences of randomly distributed primary cellular user equipments and cellular base stations by applying a Poisson point process. The network architecture consisted of multi-hop secondary devices that collect transmit energy from the fixed power beacon with a time-switching energy harvesting policy. The mutual constraints of the peak interference power, the rated power and the harvested energy were considered in this study. Two energy harvesting scenarios were performed based on the developed system model to demonstrate the effects of variable charging links. Furthermore, the end-to-end outage probability analysis expression for the half-duplex transmission scheme subject to interference from PUEs and PBSs was derived in this paper. The analytical results were validated by performing Monte Carlo simulations of the end-to-end outage probability. Moreover, the optimal charging time ratio was obtained while the maximum end-to-end transmission rate was maintained for two cases. By analyzing these two cases, it can be concluded that the charging time ratio has the most significant impact on the system performance.

Appendix I

For two EH cases, the detailed derivation processes of $W_1^{C1}(x,y)$, $W_2^{C1}(x,y)$, $W_3^{C1}(x,y)$, $W_1^{C2}(x,y)$, $W_2^{C2}(x,y)$, $W_3^{C2}(x,y)$ in (15) will be expressed as below. For case 1:

$$\begin{aligned}W_1^{C1}(x,y) &= \int_0^{\frac{R}{P_{max}}} f_D(t) f_{P_{D_i}}(x) f_A(y) \mathrm{d}t \\ &= y^{-\frac{2}{\alpha}-1}\Bigg(\exp\Bigg(\frac{4^{\frac{1}{\alpha}}\sqrt{\pi}\rho_B\Gamma\left(\frac{1}{\alpha}\right)\Gamma\left(\frac{2+\alpha}{2\alpha}\right)}{-y^{\frac{2}{\alpha}}\alpha} \\ &\quad + \frac{x d_{p,i}^{\alpha}(\tau-1)}{i\tau\eta}\Bigg) - \exp\left(\frac{\rho_B 4^{\frac{1}{\alpha}}\sqrt{\pi}\Gamma\left(\frac{1}{\alpha}\right)\Gamma\left(\frac{2+\alpha}{2\alpha}\right)}{-y^{\frac{2}{\alpha}}\alpha}\right) \\ &\quad \times \exp\left(\frac{-P_C^{\frac{2}{\alpha}}\pi d_{i-1,i}^2\rho_C}{\left(\frac{R}{P_{max}}\right)^{\frac{2}{\alpha}} P_T^{\frac{2}{\alpha}}\alpha\sin\left(\frac{1}{\alpha}\right)\cos\left(\frac{1}{\alpha}\right)}\right) \\ &\quad \times \exp\left(\frac{d_{i,i-1}^{\alpha}R}{P_{max}} + \frac{x d_{p,i}^{\alpha}(\tau-1)}{i\tau\eta}\right)\Bigg),\end{aligned} \tag{21}$$

$$\begin{aligned}W_2^{C1}(x,y) &= \int_0^{\frac{R}{x}} f_D(t) f_{P_{D_i}}(x) f_A(y) \mathrm{d}t \\ &= y^{-\frac{2}{\alpha}-1}\Bigg(\exp\left(\frac{\rho_B 4^{\frac{1}{\alpha}}\sqrt{\pi}\Gamma\left(\frac{1}{\alpha}\right)\Gamma\left(\frac{2+\alpha}{2\alpha}\right)}{-y^{\frac{2}{\alpha}}\alpha}\right) \\ &\quad \times \exp\left(\frac{-P_C^{\frac{2}{\alpha}}\pi d_{i-1,i}^2\rho_C}{\left(\frac{R}{x}\right)^{\frac{2}{\alpha}} P_T^{\frac{2}{\alpha}}\alpha\sin\left(\frac{1}{\alpha}\right)\cos\left(\frac{1}{\alpha}\right)}\right) \\ &\quad \times \exp\left(\frac{x d_{p,i}^{\alpha}(\tau-1)}{i\tau\eta} - \frac{d_{i-1,i}^{\alpha}R}{x}\right) \\ &\quad - \exp\left(\frac{\rho_B 4^{\frac{1}{\alpha}}\sqrt{\pi}\Gamma\left(\frac{1}{\alpha}\right)\Gamma\left(\frac{2+\alpha}{2\alpha}\right)}{-y^{\frac{2}{\alpha}}\alpha} + \frac{x d_{p,i}^{\alpha}(\tau-1)}{i\tau\eta}\right)\Bigg),\end{aligned} \tag{22}$$

and

$$\begin{aligned}W_3^{C1}(x,y) &= \int_0^{\frac{Ry}{I_{th}}} f_D(t) f_{P_{D_i}}(x) f_A(y) \mathrm{d}t \\ &= y^{-\frac{2}{\alpha}-1}\Bigg(-\exp\left(\frac{\rho_B 4^{\frac{1}{\alpha}}\sqrt{\pi}\Gamma\left(\frac{1}{\alpha}\right)\Gamma\left(\frac{2+\alpha}{2\alpha}\right)}{-y^{\frac{2}{\alpha}}\alpha}\right) \\ &\quad \times \exp\left(\frac{-P_C{}^{\frac{2}{\alpha}}\pi d_{i-1,i}^2\rho_C}{\left(\frac{Ry}{I_{th}}\right)^{\frac{2}{\alpha}} P_T{}^{\frac{2}{\alpha}}\alpha\sin\left(\frac{1}{\alpha}\right)\cos\left(\frac{1}{\alpha}\right)}\right) \\ &\quad \times \exp\left(\frac{x d_{p,i}^{\alpha}(\tau-1)}{i\tau\eta} - \frac{y d_{i-1,i}^{\alpha}R}{I_{th}}\right) \\ &\quad + \exp\left(\frac{x d_{p,i}^{\alpha}(\tau-1)}{i\tau\eta} - \frac{4^{\frac{1}{\alpha}}\sqrt{\pi}\rho_B\Gamma\left(\frac{1}{\alpha}\right)\Gamma\left(\frac{2+\alpha}{2\alpha}\right)}{y^{\frac{2}{\alpha}}\alpha}\right)\Bigg);\end{aligned} \tag{23}$$

for case 2, we have

$$W_1^{C2}(x,y)=\int_0^{\frac{R}{P_{max}}} f_D(t)f_{P_{D_i}}(x)f_A(y)\mathrm{d}t$$
$$=x^{i-1}y^{-\frac{2}{\alpha}-1}\Bigg(\exp\Bigg(\frac{4^{\frac{1}{\alpha}}\sqrt{\pi}\rho_B\Gamma\left(\frac{1}{\alpha}\right)\Gamma\left(\frac{2+\alpha}{2\alpha}\right)}{-y^{\frac{2}{\alpha}}\alpha}+\frac{x\alpha d_{p,i}^{\alpha}(\tau-1)}{P_b\tau\eta}\Bigg)-\exp\Bigg(\frac{\rho_B 4^{\frac{1}{\alpha}}\sqrt{\pi}\Gamma\left(\frac{1}{\alpha}\right)\Gamma\left(\frac{2+\alpha}{2\alpha}\right)}{-y^{\frac{2}{\alpha}}\alpha}\Bigg)$$
$$\times\exp\left(\frac{-P_C{}^{\frac{2}{\alpha}}\pi d_{i-1,i}^2\rho_C}{\left(\frac{R}{P_{max}}\right)^{\frac{2}{\alpha}}P_T{}^{\frac{2}{\alpha}}\alpha\sin\left(\frac{1}{\alpha}\right)\cos\left(\frac{1}{\alpha}\right)}\right)$$
$$\times\exp\left(\frac{xd_{p,i}^{\alpha}(\tau-1)}{P_b\tau\eta}-\frac{d_{i-1,i}^{\alpha}R}{P_{max}}\right)\Bigg), \tag{24}$$

$$W_2^{C2}(x,y)=\int_0^{\frac{R}{0}} f_D(t)f_{P_{D_i}}(x)f_A(y)\mathrm{d}t$$
$$=x^{i-1}y^{-\frac{2}{\alpha}-1}\Bigg(-\exp\Bigg(\frac{\rho_B 4^{\frac{1}{\alpha}}\sqrt{\pi}\Gamma\left(\frac{1}{\alpha}\right)\Gamma\left(\frac{2+\alpha}{2\alpha}\right)}{-y^{\frac{2}{\alpha}}\alpha}\Bigg)$$
$$\times\exp\left(\frac{-P_C{}^{\frac{2}{\alpha}}\pi d_{i-1,i}^2\rho_C}{\left(\frac{R}{x}\right)^{\frac{2}{\alpha}}P_T{}^{\frac{2}{\alpha}}\alpha\sin\left(\frac{1}{\alpha}\right)\cos\left(\frac{1}{\alpha}\right)}\right)$$
$$\times\exp\left(\frac{xd_{p,i}^{\alpha}(\tau-1)}{P_b\tau\eta}-\frac{d_{i-1,i}^{\alpha}R}{x}\right)$$
$$+\exp\left(\frac{4^{\frac{1}{\alpha}}\sqrt{\pi}\rho_B\Gamma\left(\frac{1}{\alpha}\right)\Gamma\left(\frac{2+\alpha}{2\alpha}\right)}{-y^{\frac{2}{\alpha}}\alpha}+\frac{d_{p,i}^{\alpha}x(\tau-1)}{P_b\tau\eta}\right)\Bigg), \tag{25}$$

and

$$W_3^{C2}(x,y)=\int_0^{\frac{Ry}{I_{th}}} f_D(t)f_{P_{D_i}}(x)f_A(y)\mathrm{d}t$$
$$=x^{i-1}y^{-\frac{2}{\alpha}-1}\Bigg(-\exp\Bigg(\frac{I_{th}\rho_B 4^{\frac{1}{\alpha}}\sqrt{\pi}\Gamma\left(\frac{1}{\alpha}\right)\Gamma\left(\frac{2+\alpha}{2\alpha}\right)}{-y^{\frac{2}{\alpha}}\alpha}\Bigg)$$
$$\times\exp\left(\frac{-P_C{}^{\frac{2}{\alpha}}\pi d_{i-1,i}^2\rho_C}{\left(\frac{Ry}{I_{th}}\right)^{\frac{2}{\alpha}}P_T{}^{\frac{2}{\alpha}}\alpha\sin\left(\frac{1}{\alpha}\right)\cos\left(\frac{1}{\alpha}\right)}\right)$$
$$\times\exp\left(\frac{xd_{p,i}^{\alpha}(\tau-1)}{P_b\tau\eta}-\frac{yd_{i-1,i}^{\alpha}R}{I_{th}}\right)$$
$$+\exp\left(\frac{4^{\frac{1}{\alpha}}\sqrt{\pi}\rho_B\Gamma\left(\frac{1}{\alpha}\right)\Gamma\left(\frac{2+\alpha}{2\alpha}\right)}{-y^{\frac{2}{\alpha}}\alpha}+\frac{d_{p,i}^{\alpha}x(\tau-1)}{P_b\tau\eta}\right)\Bigg). \tag{26}$$

REFERENCES

[1] P. K. Agyapong, M. Iwamura, D. Staehle, W. Kiess, and A. Benjebbour, "Design considerations for a 5G network architecture," *IEEE Commun. Mag.*, vol. 52, no. 11, pp. 65–75, 2014.

[2] G. A. Akpakwu, B. J. Silva, G. P. Hancke, and A. M. Abu-Mahfouz, "A survey on 5G networks for the internet of things: Communication technologies and challenges," *IEEE Access*, vol. 6, pp. 3619–3647, 2018.

[3] L. Ge, Y. Zhang, G. Chen, and J. Tong, "Compression-based lmmse channel estimation with adaptive sparsity for Massive MIMO in 5G systems," *IEEE Syst. J.*, pp. 1–11, 2019.

[4] H. Luo, Y. Zhang, W. Li, L. Huang, J. Cosmas, D. Li, C. Maple, and X. Zhang, "Low latency parallel turbo decoding implementation for future terrestrial broadcasting systems," *IEEE Trans. Broadcast.*, vol. 64, no. 1, pp. 96–104, Mar. 2018.

[5] H. Luo, Y. Zhang, L. Huang, J. Cosmas, and A. Aggoun, "A closed-loop reciprocity calibration method for Massive MIMO in terrestrial broadcasting systems," *IEEE Trans. Broadcast.*, vol. 63, no. 1, pp. 11–19, Mar. 2017.

[6] Y.-C. Liang, K.-C. Chen, G. Y. Li, and P. Mähönen, "Cognitive radio networking and communications: An overview," *IEEE Trans. Veh. Technol.*, vol. 60, no. 7, pp. 3386–3407, 2011.

[7] A. Goldsmith, S. A. Jafar, I. Maric, and S. Srinivasa, "Breaking spectrum gridlock with cognitive radios: An information theoretic perspective," *Proc. IEEE*, vol. 97, no. 5, pp. 894–914, 2009.

[8] J. Hong, B. Hong, T. W. Ban, and W. Choi, "On the cooperative diversity gain in underlay cognitive radio systems," *IEEE Trans. Commun.*, vol. 60, no. 1, pp. 209–219, 2012.

[9] J. Lee, H. Wang, J. G. Andrews, and D. Hong, "Outage probability of cognitive relay networks with interference constraints," *IEEE Trans. Wireless Commun.*, vol. 10, no. 2, pp. 390–395, 2011.

[10] G. Chen, Z. Tian, Y. Gong, and J. Chambers, "Decode-and-forward buffer-aided relay selection in cognitive relay networks," *IEEE Trans. Veh. Technol.*, vol. 63, no. 9, pp. 4723–4728, Nov. 2014.

[11] D. S. Gurjar, H. H. Nguyen, and H. D. Tuan, "Wireless information and power transfer for IoT applications in overlay cognitive radio networks," *IEEE Internet Things J.*, vol. 6, no. 2, pp. 3257–3270, Apr. 2019.

[12] S. Haykin *et al.*, "Cognitive radio: brain-empowered wireless communications," *IEEE J. Sel. Areas Commun.*, vol. 23, no. 2, pp. 201–220, 2005.

[13] G. Chen, J. Tang, and J. P. Coon, "Optimal routing for multihop social-based D2D communications in the internet of things," *IEEE Internet Things J.*, vol. 5, no. 3, pp. 1880–1889, Jun. 2018.

[14] C. Sexton, Q. Bodinier, A. Farhang, N. Marchetti, F. Bader, and L. A. DaSilva, "Enabling asynchronous machine-type D2D communication using multiple waveforms in 5G," *IEEE Internet Things J.*, vol. 5, no. 2, pp. 1307–1322, Apr. 2018.

[15] X. Liu, Z. Li, N. Zhao, W. Meng, G. Gui, Y. Chen, and F. Adachi, "Transceiver design and multihop D2D for UAV IoT coverage in disasters," *IEEE Internet Things J.*, vol. 6, no. 2, pp. 1803–1815, Apr. 2019.

[16] G. Chen, J. P. Coon, A. Mondal, B. Allen, and J. A. Chambers, "Performance analysis for multihop full-duplex IoT networks subject to poisson distributed interferers," *IEEE Internet Things J.*, vol. 6, no. 2, pp. 3467–3479, Apr. 2019.

[17] G. Fodor, E. Dahlman, G. Mildh, S. Parkvall, N. Reider, G. Miklós, and Z. Turányi, "Design aspects of network assisted device-to-device communications," *IEEE Commun. Mag.*, vol. 50, no. 3, 2012.

[18] Y. Li, Y. Liang, Q. Liu, and H. Wang, "Resources allocation in multicell D2D communications for internet of things," *IEEE Internet Things J.*, vol. 5, no. 5, pp. 4100–4108, Oct. 2018.

[19] J. Sachs, I. Mari, and A. Goldsmith, "Cognitive cellular systems within the TV spectrum," *Proc. IEEE DySPAN*, pp. 1–12, 2010.

[20] A. Sultana, L. Zhao, and X. Fernando, "Efficient resource allocation in device-to-device communication using cognitive radio technology," *IEEE Trans. Veh. Technol.*, vol. 66, no. 11, pp. 10 024–10 034, Nov. 2017.

[21] S. Dang, G. Chen, and J. P. Coon, "Outage performance analysis of full-duplex relay-assisted device-to-device systems in uplink cellular networks," *IEEE Trans. Veh. Technol.*, vol. 66, no. 5, pp. 4506–4510, May 2017.

[22] A. Sultana, L. Zhao, and X. Fernando, "Energy-efficient power allocation in underlay and overlay cognitive device-to-device communications," *IET Communications*, vol. 13, no. 2, pp. 162–170, 2019.

[23] J. Lee and J. H. Lee, "Performance analysis and resource allocation for cooperative D2D communication in cellular networks with multiple D2D pairs," *IEEE Commun. Lett.*, vol. 23, no. 5, pp. 909–912, May 2019.

[24] V. Petrov, A. Samuylov, V. Begishev, D. Moltchanov, S. Andreev, K. Samouylov, and Y. Koucheryavy, "Vehicle-based relay assistance for opportunistic crowdsensing over narrowband IoT (NB-IoT)," *IEEE Internet Things J.*, vol. 5, no. 5, pp. 3710–3723, Oct 2018.

[25] D. S. Gurjar and P. K. Upadhyay, "Overlay Device-to-Device communications in asymmetric two-way cellular systems with hybrid relaying," *IEEE Syst. J.*, vol. 12, no. 4, pp. 3713–3724, Dec. 2018.

[26] J. Tang, G. Chen, and J. P. Coon, "Route selection based on connectivity-delay-trust in public safety networks," *IEEE Syst. J.*, vol. 13, no. 2, pp. 1558–1567, Jun. 2019.

[27] S. Cho, B. Spencer, H. Jo, J. Li, and R. E. Kim, "Bridge monitoring using wireless smart sensors," *SPIE Newsroom*, pp. 1–3, 2012.

[28] L. Jiang, H. Tian, Z. Xing, K. Wang, K. Zhang, S. Maharjan, S. Gjessing, and Y. Zhang, "Social-aware energy harvesting device-to-device communications in 5G networks," *IEEE Wireless Communications*, vol. 23, no. 4, pp. 20–27, 2016.

[29] K. Janghel and S. Prakriya, "Throughput of underlay cognitive energy harvesting relay networks with an improved time-switching protocol," *IEEE Trans. Cogn. Commun. Netw.*, vol. 4, no. 1, pp. 66–81, Mar. 2018.

[30] G. Chen, P. Xiao, J. R. Kelly, B. Li, and R. Tafazolli, "Full-duplex wireless-powered relay in two way cooperative networks," *IEEE Access*, vol. 5, pp. 1548–1558, 2017.

[31] Y. Gu and S. Aïssa, "RF-based energy harvesting in decode-and-forward relaying systems: Ergodic and outage capacities," *IEEE Trans. Wireless Commun.*, vol. 14, no. 11, pp. 6425–6434, Nov. 2015.

[32] K. B. Letaief, W. Chen, Y. Shi, J. Zhang, and Y. A. Zhang, "The roadmap to 6G: AI empowered wireless networks," *IEEE Commun. Mag*, vol. 57, no. 8, pp. 84–90, August 2019.

[33] N. Ashraf, A. Hasan, H. K. Qureshi, and M. Lestas, "Combined data rate and energy management in harvesting enabled tactile IoT sensing devices," *IEEE Trans. Ind. Informat.*, vol. 15, no. 5, pp. 3006–3015, May 2019.

[34] M. Haenggi, *Stochastic geometry for wireless networks*. Cambridge University Press, 2012.

[35] A. H. Sakr and E. Hossain, "Cognitive and energy harvesting-based D2D communication in cellular networks: Stochastic geometry modeling and analysis," *IEEE Trans. Commun.*, vol. 63, no. 5, pp. 1867–1880, 2015.

[36] Y. Liu, L. Wang, S. A. Raza Zaidi, M. Elkashlan, and T. Q. Duong, "Secure D2D communication in large-scale cognitive cellular networks: A wireless power transfer model," *IEEE Trans. Commun.*, vol. 64, no. 1, pp. 329–342, Jan. 2016.

[37] M. M. Mansour and H. Kanaya, "High-efficient broadband CPW RF rectifier for wireless energy harvesting," *IEEE Microw. Wireless Compon. Lett.*, vol. 29, no. 4, pp. 288–290, Apr. 2019.

[38] M. Qiu, Y. Huang, and J. Yuan, "Downlink non-orthogonal multiple access without SIC for block fading channels: An algebraic rotation approach," *IEEE Trans. Wireless Commun.*, vol. 18, no. 8, pp. 3903–3918, Aug 2019.

[39] M. Hofer, Z. Xu, D. Vlastaras, B. Schrenk, D. Löschenbrand, F. Tufvesson, and T. Zemen, "Real-Time geometry-based wireless channel emulation," *IEEE Trans. Veh. Technol.*, vol. 68, no. 2, pp. 1631–1645, Feb 2019.

[40] G. Amos and V. Subramaniam, "Numerical methods for engineers and scientists: An introduction with applications using MATLAB," *Department of Mechanical Engineering. The Ohio State University. Ohio, USA*, 2014.